Electronic Supplementary Material (ESI) for RSC Advances.

Supporting Information

High-Performance Electrocatalyst for Oxygen Reduction Reaction Derived from Copolymer Networks and Iron(II) Acetate

Mei Yang [a], Hongbiao Chen [a]*, Duanguang Yang [a], Yong Gao [a], Huaming Li [a, b]*

[a] College of Chemistry, Xiangtan University, Xiangtan 411105, Hunan Province, P. R. China.

[b] Key Laboratory of Polymeric Materials & Application Technology of Hunan Province, and Key Laboratory of Advanced Functional Polymeric Materials of College of Hunan Province, Xiangtan University, Xiangtan 411105, Hunan Province, P. R. China.

*Corresponding authors. Tel.: +86 731 58298572; Fax: +86 731 58293264.

E-mail address: lihuaming@xtu.edu.cn (H. Li), chhb606@163.com (H. Chen)

Supporting Information Contains:

S1. Materials

Pyrrole, cyanuryl chloride, formaldehyde dimethyl acetal (FDA), ferric chloride ($FeCl_3$) and iron(II) acetate ($Fe(OAc)_2$) were purchased from Shanghai Aladdin Industrial Co., (China). Pyrrole was purified by distillation in *vacuo*. 1, 2-Dichloroethane was dried by anhydrous $CaCl_2$ followed by distillation in *vacuo*. All other reagents were used as received.

S2. Instruments

The textural properties were characterized by N_2 sorption measurements at 77 K (Micromeritics TriStar II 3020). The specific surface area was obtained by Brunauer- Emmett-Teller (BET) method. The pore size distribution (PSD) was calculated from the adsorption branches of the isotherms using the Barrett-Joyner-Halenda (BJH) model. The total pore volume (V_{total}) was estimated from the adsorbed amount at a relative pressure P/P_o of 0.99. Micropore volume (V_{mic}) was calculated using the t-plot method. Scanning electron microscopy (SEM) images were recorded using S-4800 (JEOL) operated at an acceleration voltage of 10 kV. The transmission electron microscopy (TEM) images were recorded on a JEOL JEM-1011 transmission electron microscope (Japan) operating at 200 kV. High-resolution TEM (HRTEM) was performed using a JEM-2100F Atomic Resolution Analytical Microscope operating at an accelerating voltage of 200 kV. The X-ray photoelectron spectroscopy (XPS) was performed on a K-Alpha 1063 photoelectron spectrometer (Thermo Fisher Scientific, England) with Al-Kα X-ray radiation as the X-ray source for excitation. Inductively coupled plasma atomic emission spectrometry (ICP-AES)

analyses were carried out on a Perkin Elmer Optima 5300 DV spectrometer. Raman spectra were recorded using a Renishaw inVia Raman spectrometer at 25 °C. The spectral were recorded over the range of 200−3200 cm^{-1} using the 532 nm emission of a Ar ion laser source, and the resolution was 1 cm^{-1}. Samples were prepared by gently pressing Fe-N_{TP}/Cs fine powders into a flat thin film on glass substrate, and each sample was recorded randomly on three different positions.

S3. Electrochemical performance of Fe-N_{TP}/Cs

Tafel slope calculated by linear regression method, the mass transport corrected ORR specific kinetic current density ($\boldsymbol{i}_{\mathbf{kinetic}}$) was calculated by the following equation:

$$\boldsymbol{i}_{\mathbf{kinetic}} = (\boldsymbol{i}_{\mathbf{limited}} * \boldsymbol{i}_{\mathbf{measured}}) / (\boldsymbol{i}_{\mathbf{limited}} - \boldsymbol{i}_{\mathbf{measured}})$$

where $\boldsymbol{i}_{\mathbf{kinetic}}$ [mA cm^{-2}] is the Faradic current, $\boldsymbol{i}_{\mathbf{limited}}$ [mA cm^{-2}] is the limiting current density, and $\boldsymbol{i}_{\mathbf{measured}}$ [mA cm^{-2}] is the current density measured.

The Koutecky-Levich plots were obtained by linear fitting of the reciprocal rotating speed versus reciprocal current density collected at different potentials. The overall electron transfer numbers (n) per oxygen molecule involved in a typical ORR process were calculated from the slopes of Koutecky-Levich plots using the following equation:

$$1/J = 1/J_k + 1/(B\omega^{1/2})$$

Where J is the measured current density, J_k is the kinetic current density, ω is the electrode rotating speed in rpm, and B, the reciprocal of the slope, which was determined from the slope of Koutecky-Levich plots based on Levich equation as followed:

$$B = 0.2nFv^{-1/6}C_{O2}D_{O2}^{2/3}$$

Where n is the number of electrons transferred per oxygen molecule, F is the Faraday constant (96485 C mol^{-1}). The diffusion coefficient of oxygen D_{O2} in 0.1 M $HClO_4$ is 1.9×10^{-5} cm^2 s^{-1} (1.98×10^{-5} cm^2 s^{-1} in 0.1 M KOH), v is the kinetic viscosity (0.01 cm^2 s^{-1}), and the concentration of oxygen C_{O2} is 1.2×10^{-3} mol L^{-1} (1.48×10^{-3} mol L^{-1} in 0.1 M KOH). The constant 0.2 is adopted when the rotating speed is in rpm.

Rotating ring-disk electrode (RRDE) measurements was carried out to determine the four-electron selectivity. Before the experiments, the Pt ring electrode was activated through CV in 0.5 M $HClO_4$ from –0.2 to 1.0 V vs. Ag/AgCl at a scan rate of 100 mV s^{-1} for 10 minutes. For measurements, the disk electrode was scanned at a rate of 10 mV s^{-1}, and the ring electrode potential was set to 0.4 V and 1.1 V (vs. Ag/AgCl) in 0.1 M KOH and 0.1 M $HClO_4$, respectivily. The Hydrogen peroxide yield ($\%H_2O_2$) and the electron transfer number (n) were calculated by the followed equations:

$$\%H_2O_2 = 200 \times \frac{i_r / N}{i_r / N + i_d}$$

$$n = 4 \times \frac{i_d}{i_r / N + i_d}$$

where i_d and i_r are the disk and ring currents, respectively. N is the ring current collection efficiency which was determined to be 37% by the reduction of 10 mM $K_3[Fe(CN)_6]$ in 0.1 M KNO_3.

S4. Synthesis of 2,4,6-tripyrrol-1,3,5-triazine (TPT)

TPT was prepared according to the procedure reported previously by our group.[1] In a typical

experiment, to an ice-cold solution of pyrrole (6.78 g, 0.10 mol) in 80 mL of anhydrous tetrahydrofuran, KOH (8.86 g, 0.15 mol) was added. After stirring at room temperature for 3 h, cyanuryl chloride (5.59 g, 0.03 mol) was added portion-wise. The reaction mixture was then stirred at room temperature for another 18 h. The reaction was then quenched by the addition of 250 mL iced water and the precipitate was filtered, washed with distilled water (3 × 200 mL), and dried in a vacuum oven at 80 °C for 24 h. The crude product was recrystallized from acetone and ethanol mixed solvent (80/20, v/v), giving TPT in 56% yield (4.64 g).

S5. Synthesis of polymeric networks

S5-1. Synthesis of TPT-Py CPN

In a typical procedure, to a solution of TPT (0.01 mol), pyrrole (0.03 mol) and FDA (0.12 mol) in anhydrous 1,2-dichloroethane (DCE, 300 mL), ferric chloride ($FeCl_3$, 0.12 mol) was added under nitrogen atmosphere. The mixture was heated at 45 °C for 5 h and then at 80 °C for 19 h. In all cases, a solid precipitated quickly from the reaction mixture. The material was collected and thoroughly washed with methanol to remove the remaining catalyst and unconsumed monomer. Further purification was carried out by Soxhlet extraction with methanol for 48 h and drying at 60 °C to a constant mass.

S5-2. Synthesis of TPT PN

For the synthesis of TPT PN, the molar ratio of TPT, FDA and $FeCl_3$ is 1: 6: 6, the other reaction conditions are the same as the optimization conditions of the synthesis of TPT-Py CPN.

S5-3. Synthesis of Py PN

For the synthesis of Py PN, the molar ratio of Py, FDA and $FeCl_3$ is 1: 2: 2, the other reaction conditions are the same as the optimization conditions of the synthesis of TPT-Py CPN.

S6. Effect of TPT/Py molar ratio

A series of TPT-Py CPN samples of different TPT/Py molar ratio (TPT/Py = 1:1, 1:3, 1:5) was prepared. In a typical procedure, to a solution of TPT (0.01 mol), pyrrole (0.01-0.05 mol) and FDA (0.08-0.16 mol) in anhydrous 1,2-dichloroethane (DCE, 300 mL), ferric chloride ($FeCl_3$, 0.08-0.16 mol) was added under nitrogen atmosphere. The mixture was heated at 45 °C for 5 h and then at 80 °C for 19 h. In all cases, a solid precipitated quickly from the reaction mixture. The material was collected and thoroughly washed with methanol to remove the remaining catalyst and unconsumed monomer. Further purification was carried out by Soxhlet extraction with methanol for 48 h. The products are denoted as TPT-Py CPN-1, TPT-Py CPN-3, and TPT-Py CPN-5, respectively, for TPT/Py molar ratio of 1/1, 1/3, and 1/5.

To simplify the study, the pyrolysis temperature was fixed at 900 °C. Firstly, 350 mg of TPT-Py CPN-1, TPT-Py CPN-3, and TPT-Py CPN-5 were separately mixed with $Fe(OAc)_2$ (100 mg) in ethanol for 3 h. The suspensions were spread onto an evaporating dish and dried. The mixtures

were then separately placed into a ceramic tube and pyrolyzed at 900 °C for 1 h in Ar with a heating rate of 4 °C min^{-1}. To remove a redundant phase, mainly unreacted metallic iron and iron compounds, the composites were preleached in 0.5 M H_2SO_4 at 80 °C for 24 h. In the final step, each composite was heat-treated for a second time at 900 °C for 1 h in Ar, and the products are denoted as Fe-N_{TP}/C-900/1, Fe-N_{TP}/C-900/3, Fe-N_{TP}/C-900/5, respectively, for TPT/Py molar ratio of 1/1, 1/3, and 1/5.

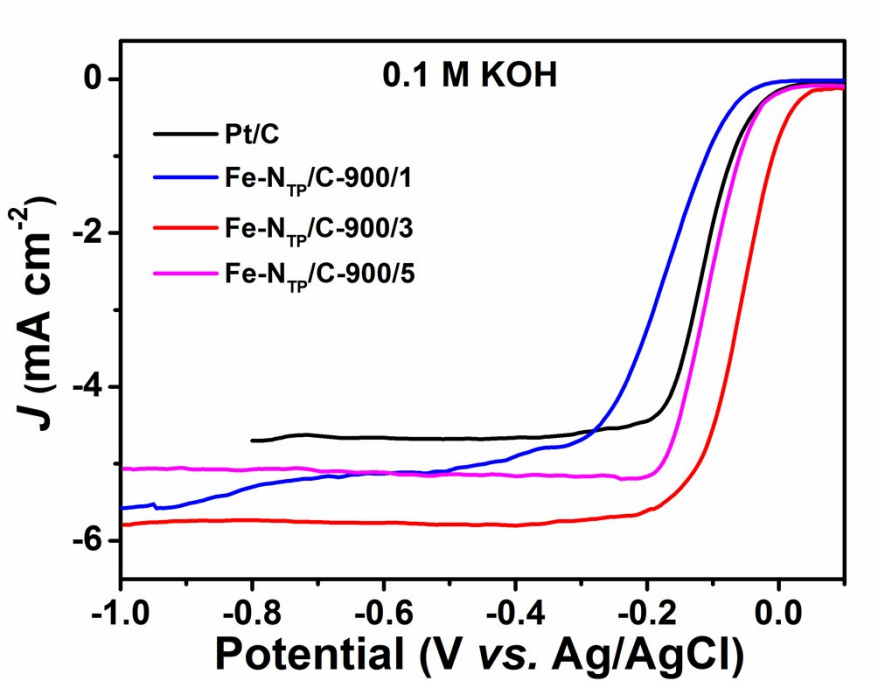

Figure S1. RDE voltammograms of catalysts prepared from different TPT/Py molar ratio in O_2-saturated 0.1 M KOH with the rotation speed of 1600 rpm.

Table S1. Electrochemical properties of the Fe-N_{TP}/C-900/1-5 catalysts.

Sample	TPT/Py (mol/mol)	E_o [a] (V)	$E_{1/2}$ [b] (V)	J_L [c] (mA cm^{-2})
Fe-N_{TP}/C-900/1	1/1	−0.034	−0.180	5.30

Fe-N_{TP}/C-900/3	1/3	0.051	−0.055	5.79
Fe-N_{TP}/C-900/5	1/5	0.008	−0.105	5.07

[a] Onset potential in O_2 saturated 0.1 M KOH solution with the rotation speed of 1600 rpm.

[b] Half-wave potential in O_2 saturated 0.1 M KOH solution with the rotation speed of 1600 rpm.

[c] Limiting current density in O_2 saturated 0.1 M KOH solution at −0.8 V.

S7. Effect of Fe loadings

To determine the optimum Fe loading, catalysts with different iron loadings were prepared under optimal TPT/Py molar ratio (TPT/Py = 1:3). To simplify the study, the pyrolysis temperature was fixed at 900 °C. The detailed procedure is as follows: $Fe(OAc)_2$ and TPT-Py CPN mixtures with mass ratio of 5/35, 10/35, 20/35, and 40/35, were separately sonicated (60 W) in ethanol at ambient temperature for 180 min. The resulting suspensions were evaporated to dryness and dried. The mixtures were then separately placed into a ceramic tube and pyrolyzed at 900 °C for 1 h in Ar with a heating rate of 4 °C min^{-1}. The composites were preleached in 0.5 M H_2SO_4 at 80 °C for 24 h. In the final step, the composites were heat-treated for a second time at 900 °C for 1 h in Ar, the products are denoted as Fe-N_{TP}/C-900-1, Fe-N_{TP}/C-900-2, Fe-N_{TP}/C-900-3, and Fe-N_{TP}/C-900-4, respectively, for $Fe(OAc)_2$/TPT-Py CPN mass ratio of 5/35, 10/35, 20/35, and 40/35.

Figure S2 shows the RDE voltammograms of catalysts with different iron loadings in O_2-saturated 0.1 M KOH with the rotation speed of 1600 rpm. As shown in **Table S2**, the ORR activity of electrocatalysts increase with the Fe loading, go through a maximum at 0.875 wt%, then decrease at higher Fe loadings. This may be due to the formation of crystalline particles, which do not

contribute to the oxygen reduction activity.

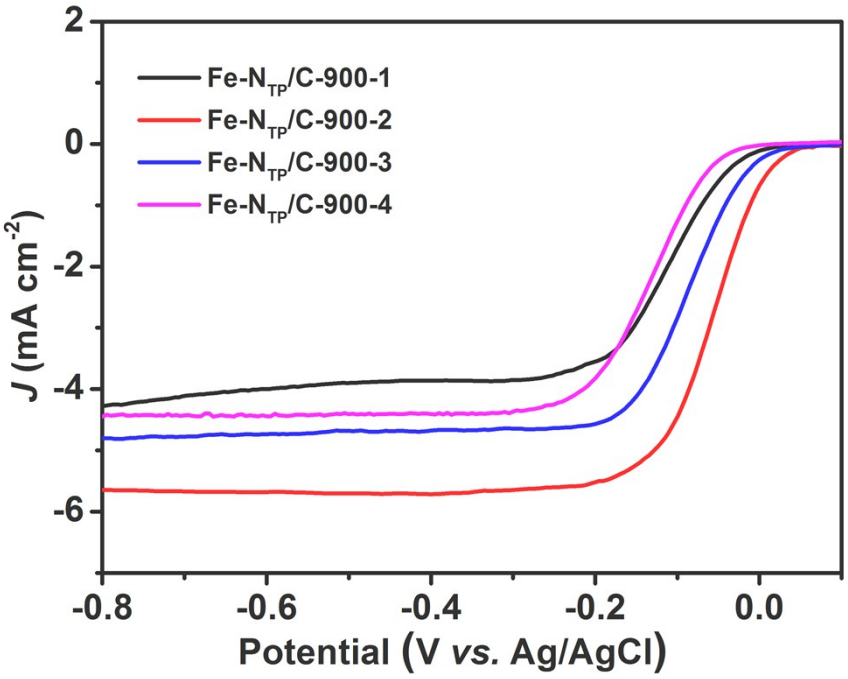

Figure S2. RDE voltammograms of catalysts prepared from different $Fe(OAc)_2$/TPT-Py CPN mass ratios in O_2-saturated 0.1 M KOH with the rotation speed of 1600 rpm.

Table S2. Electrochemical properties of the electrocatalysts with different Fe loadings.

Sample	$Fe(OAc)_2$ (mg)	TPT-Py CPN (mg)	Fe contents [a] (wt%)	E_o [b] (V)	J_L [c] (mA cm^{-2})
Fe-N$_{TP}$/C-900-1	50	350	0.516	0.030	4.27

Fe-N_{TP}/C-900-2	100	350	0.875	0.051	5.79
Fe-N_{TP}/C-900-3	200	350	1.485	0.029	4.80
Fe-N_{TP}/C-900-4	400	350	2.150	−0.020	4.45

[a] Determined by ICP-AES analysis.

[b] ORR onset potential in O_2 saturated 0.1 M KOH solution with the rotation speed of 1600 rpm.

[c] Limiting current density in O_2 saturated 0.1 M KOH solution at −0.8 V.

S8. Effect of pyrolysis temperatures

TPT-Py CPN (1050 mg) and $Fe(OAc)_2$ (300 mg) were sonicated (60 W) in ethanol (360 mL) at ambient temperature for 180 min. Then, the solvent was evaporated at 60 °C and dried, forming a uniform solid mixture. The mixture was divided into three portions of 450 mg and then separately placed into a ceramic tube and pyrolyzed at 800 °C, 900 °C, and 1000 °C for 1 h in Ar with a heating rate of 4 °C min^{-1}. To remove a redundant phase, mainly unreacted metallic iron and iron compounds, the composites were preleached in 0.5 M H_2SO_4 at 80 °C for 24 h. In the final step, the composites were heat-treated for a second time at 900 °C for 1 h in Ar, and the products are denoted as Fe-N_{TP}/C-800, Fe-N_{TP}/C-900, and Fe-N_{TP}/C-1000, respectively. **Figure S3** shows the RDE voltammograms of Fe-N_{TP}/C-800, Fe-N_{TP}/C-900, and Fe-N_{TP}/C-1000 in O_2-saturated 0.1 M KOH with the rotation speed of 1600 rpm. **Figure S4** shows the CVs for these electrocatalysts in O_2-saturated 0.1 M KOH aqueous solution at a scan rate of 50 mV s^{-1}. **Table S3** shows the ORR peak currents, ORR peak potentials, ORR onset potential, and Limiting current density for Fe-N_{TP}/C-800, Fe-N_{TP}/C-900, and Fe-N_{TP}/C-1000.

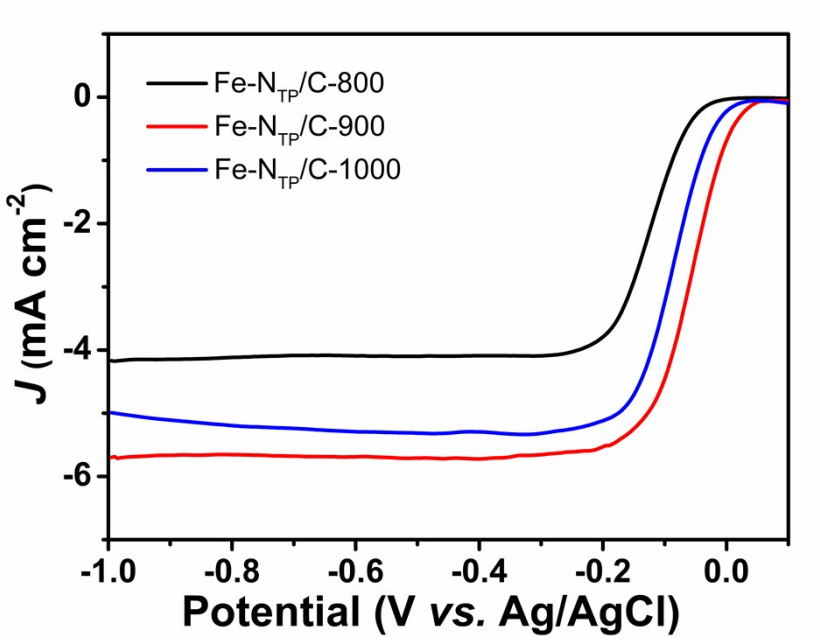

Figure S3. RDE voltammograms of Fe-N_{TP}/C-800, Fe-N_{TP}/C-900, and Fe-N_{TP}/C-1000 in O_2-saturated 0.1 M KOH with the rotation speed of 1600 rpm.

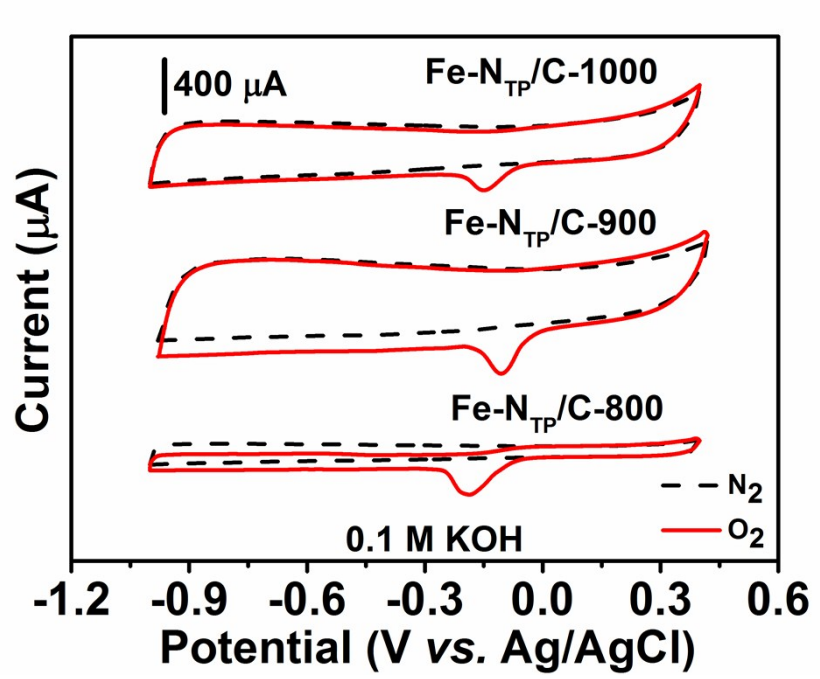

Figure S4. CV curves for Fe-N_{TP}/C-800, Fe-N_{TP}/C-900, and Fe-N_{TP}/C-1000 in O_2-saturated 0.1 M KOH at a scan rate of 50 mV s^{-1}.

Table S3. Electrochemical properties of Fe-N_{TP}/C-800, Fe-N_{TP}/C-900, and Fe-N_{TP}/C-1000.

Samples	Temperatures (°C)	Peak potentials (V *vs.* Ag/AgCl)	Peak currents (μA)	E_o [a] (V)	J_L [b] (mA cm^{-2})
Fe-N_{TP}/C-800	800	–0.19	278	0.005	4.12
Fe-N_{TP}/C-900	900	–0.11	325	0.051	5.79
Fe-N_{TP}/C-1000	1000	–0.17	192	0.042	5.20

[a] ORR onset potential in O_2 saturated 0.1 M KOH solution with the rotation speed of 1600 rpm.

[b] Limiting current density in O_2 saturated 0.1 M KOH solution at −0.8 V.

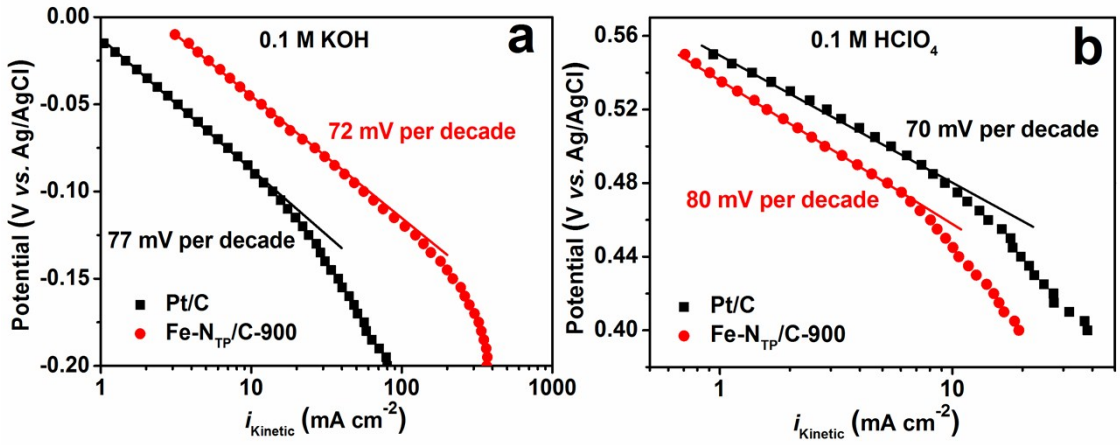

Figure S5. Tafel plots for Fe-N_{TP}/C-900 and Pt/C in an O_2-saturated 0.1 M KOH (a) and 0.1 M $HClO_4$ (b).

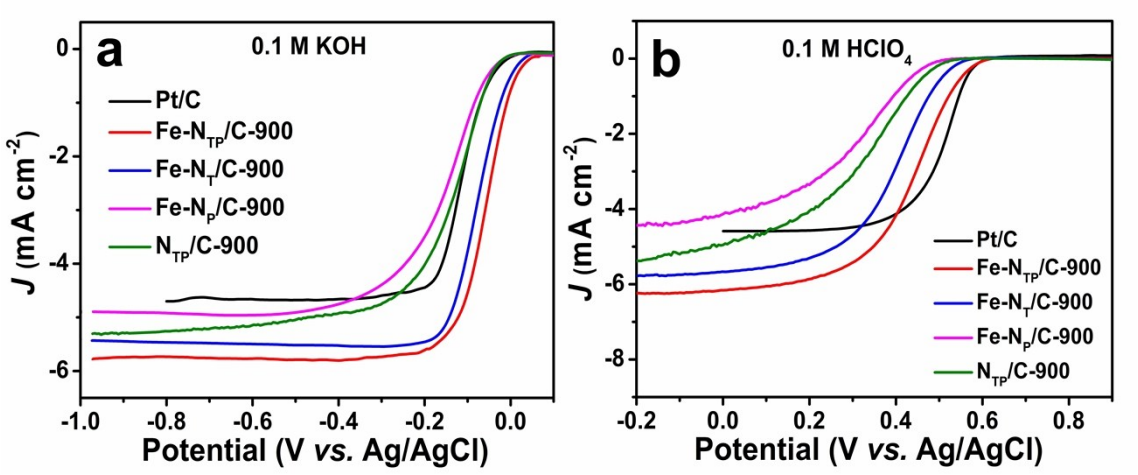

Figure S6. RDE voltammograms of Fe−N_{TP}/C-900, Fe−N_T/C-900, Fe−N_P/C-900, N_{TP}/C-900 and Pt/C in O_2-saturated 0.1 M KOH (a) and 0.1 M $HClO_4$ (b).

Table S4. Electrochemical properties for Fe−N_{TP}/C-900, Fe−N_T/C-900, Fe−N_P/C-900, N_{TP}/C-900 and Pt/C catalysts.

Samples	E_o (V) [a]		$E_{1/2}$ (V) [b]		J_L (mA cm^{-2}) [c]	
	0.1 M KOH	0.1 M $HClO_4$	0.1 M KOH	0.1 M $HClO_4$	0.1 M KOH	0.1 M $HClO_4$
Pt/C	0.001	0.620	−0.120	0.500	5.41	5.27
Fe−N_{TP}/C-900	0.051	0.605	−0.055	0.445	5.79	6.12
Fe−N_T/C-900	0.041	0.570	−0.070	0.430	5.52	5.62

Fe−N_P/C-900	−0.004	0.530	−0.145	0.340	4.92	4.05
N_{TP}/C-900	−0.001	0.540	−0.127	0.360	5.30	5.25

[a] Onset potential; [b] Half-wave potential; [c] Limiting current density obtained at –0.8 V in O_2-saturated 0.1 M KOH solution and at +0.0 V in O_2-saturated 0.1 M $HClO_4$ solution with the rotation speed of 1600 rpm.

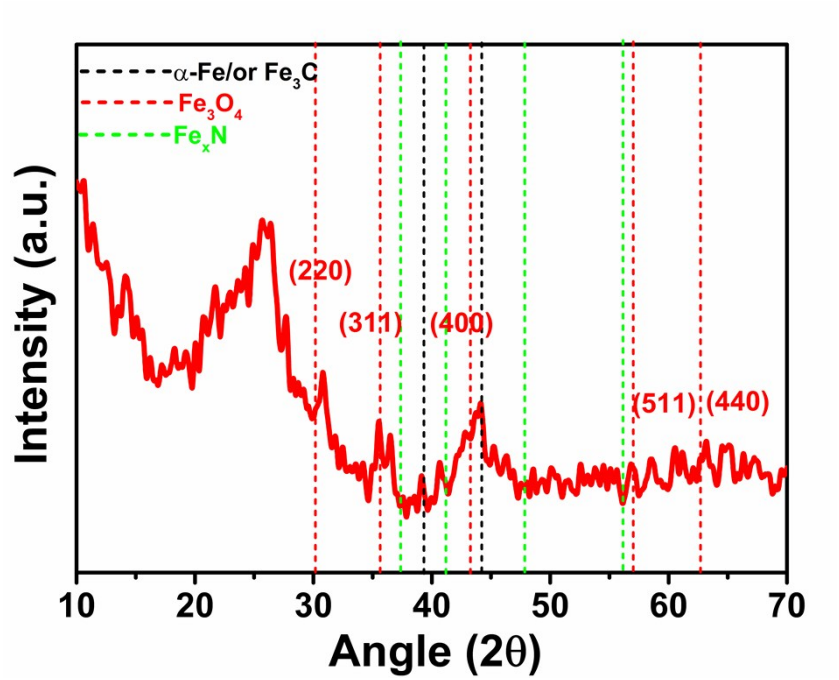

Figure S7. X-ray diffractograms of Fe-N_{TP}/C-900.

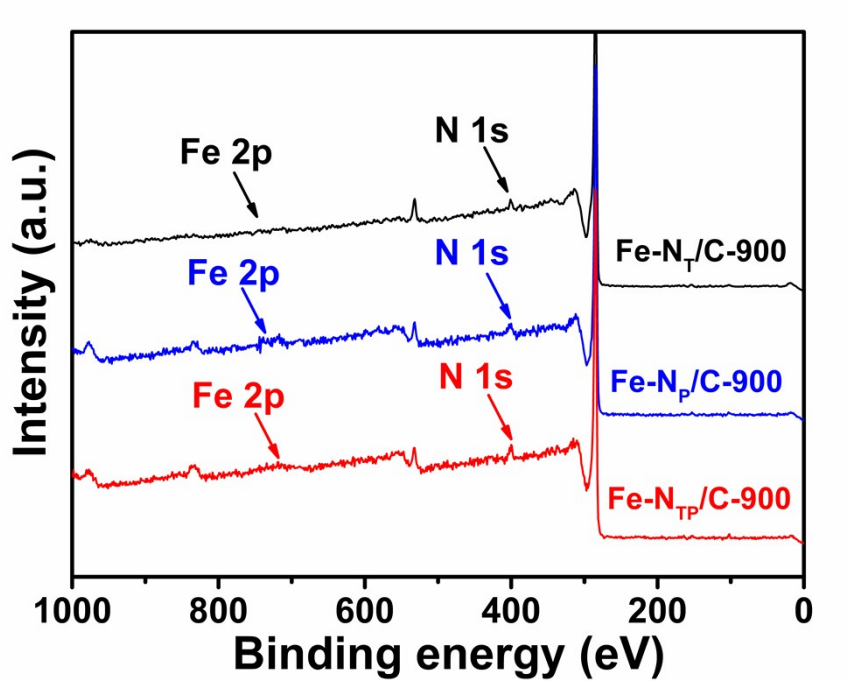

Figure S8. XPS survey scan of Fe-N_{TP}/C-900, Fe-N_T/C-900 and Fe-N_P/C-900 catalysts.

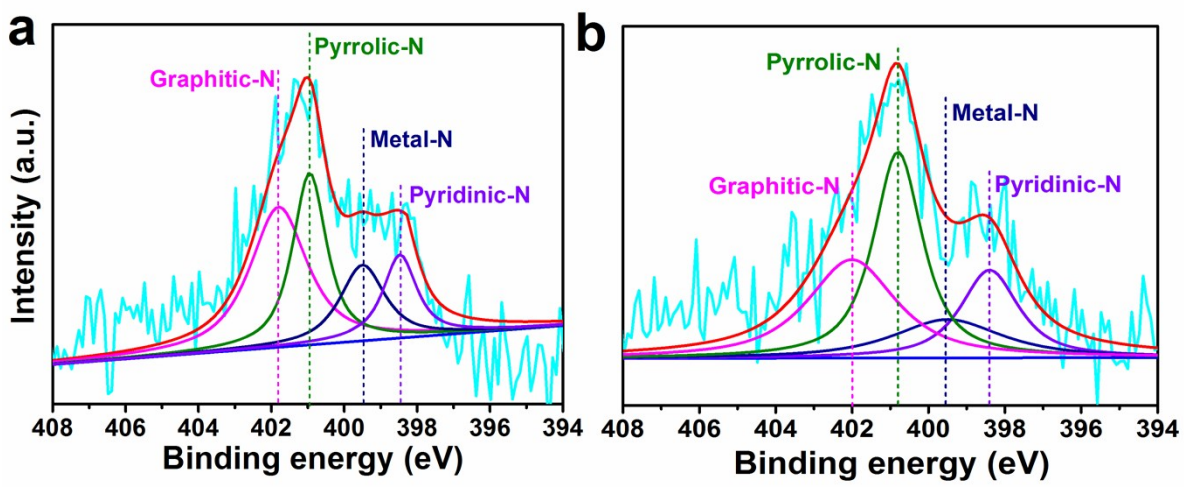

Figure S9. N 1s XPS spectra of Fe-N_T/C-900 (a) and Fe-N_P/C-900 catalysts (b).

Table S5. Elemental composition of Fe-N_{TP}/C-900, Fe-N_T/C-900 and Fe-N_P/C-900 by XPS.

Samples	C (at. %)	O (at. %)	N (at. %)	Fe (at. %)	Fe [a] (wt %)
Fe-N_{TP}/C-900	93.66	3.59	2.59	0.16	0.875
Fe-N_T/C-900	94.00	3.80	2.10	0.10	0.595
Fe-N_P/C-900	94.25	3.30	2.03	0.42	2.789

[a] Fe contents of Fe-N_{TP}/C-900, Fe-N_T/C-900 and Fe-N_P/C-900 catalysts measured by ICP-AES.

Table S6. The distribution of N species obtained from the de-convolution of the N 1s peaks of Fe-N_{TP}/C-900, Fe-N_T/C-900 and Fe-N_P/C-900 catalysts.

Samples	N (at. %)	N1 [a] (398.5 eV) (%)	N2 [b] (399.8 eV) (%)	N3 [c] (400.7 eV) (%)	N4 [d] (401.4 eV) (%)
Fe-N_{TP}/C-900	2.59	21.96	16.78	27.22	34.04
Fe-N_T/C-900	2.10	12.86	17.62	29.52	40.00
Fe-N_P/C-900	2.03	18.23	14.78	35.96	31.03

[a] Pyridinic-N. [b] Fe-N. [c] Pyrrolic-N. [d] Graphitic-N.

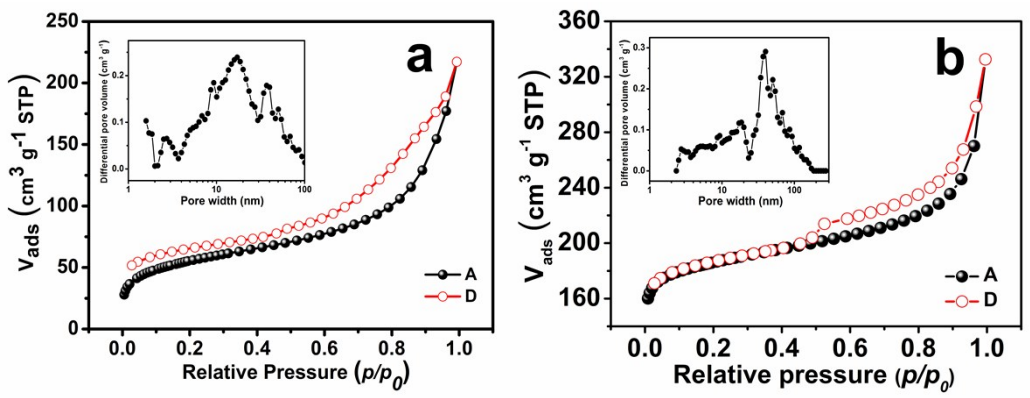

Figure S10. Nitrogen adsorption (closed)/desorption (open) isotherms for TPT-Py CPN (a) and Fe-N_{TP}/C-900 (b) at 77 K, the inset shows the pore size distribution for TPT-Py CPN (a) and Fe-N_{TP}/C-900 (b).

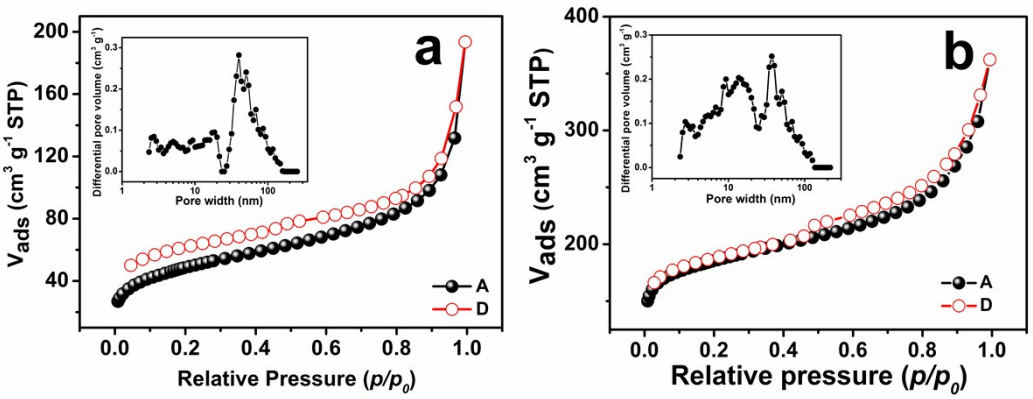

Figure S11. Nitrogen adsorption (closed)/desorption (open) isotherms for TPT PN (a) and Fe-N_T/C-900 (b) at 77 K, the inset shows the pore size distribution for TPT PN (a) and Fe-N_T/C-900 (b).

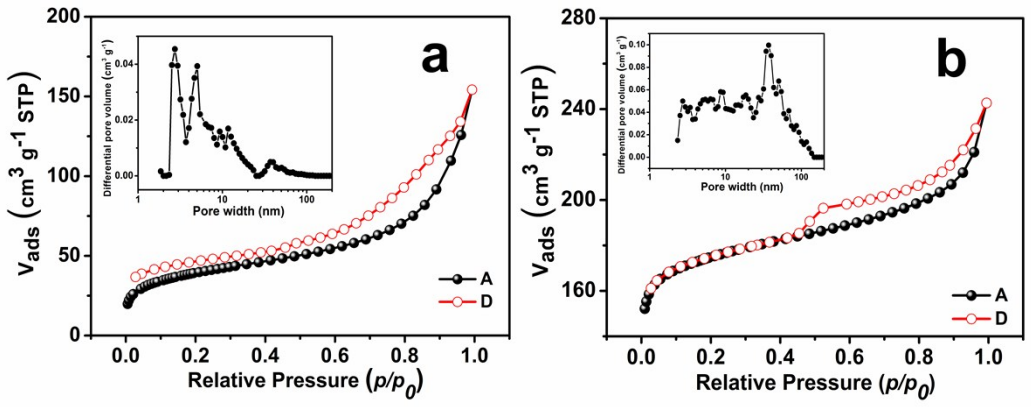

Figure S12. Nitrogen adsorption (closed)/desorption (open) isotherms for Py PN (a) and Fe-N_P/C-900 (b) at 77 K, the inset shows the pore size distribution for Py PN (a) and Fe-N_P/C-900 (b).

Table S7. Textural Properties of Fe-N_{TP}/C-900, Fe-N_T/C-900, Fe-N_P/C-900 catalysts and their precursor.

Samples	S_{BET} ($m^2\ g^{-1}$)	D_a [a] (nm)	V_{total} [b] ($cm^3\ g^{-1}$)	V_{mic} [c] ($cm^3\ g^{-1}$)	V_{mic}/V_{total} (%)
TPT-Py CPN	205	6.55	0.336	0.020	5.95
TPT PN	177	6.77	0.299	0.032	10.70
Py PN	145	2.91	0.283	0.029	9.76
Fe-N_{TP}/C-900	724	2.84	0.514	0.247	48.10
Fe-N_T/C-900	710	3.16	0.560	0.230	41.10
Fe-N_P/C-900	683	2.20	0.375	0.242	64.50

[a] Average pore diameter. [b] Total pore volume. [c] Micropore volume.

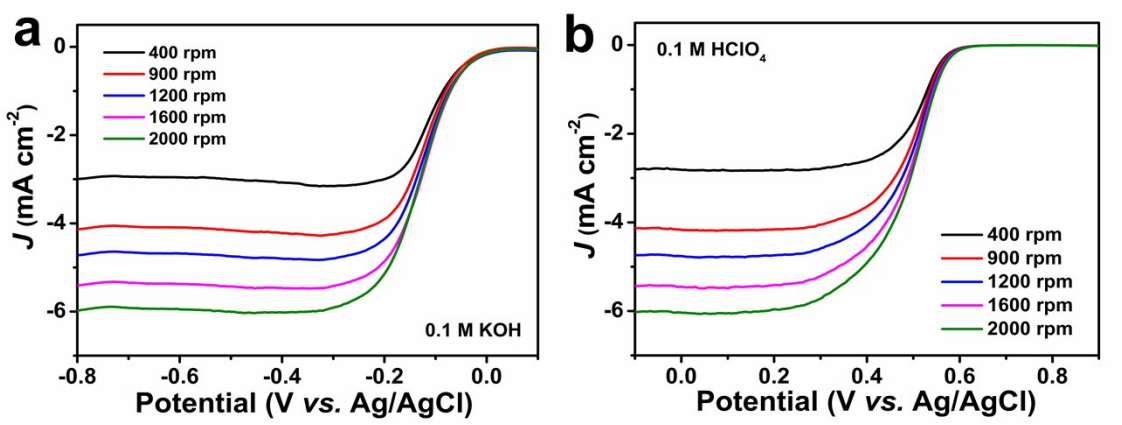

Figure S13. LSV curves of Pt/C in O_2-saturated 0.1 M KOH (a) and 0.1 M $HClO_4$ (b) with a sweep rate of 10 mV s^{-1} at the different rotation rates.

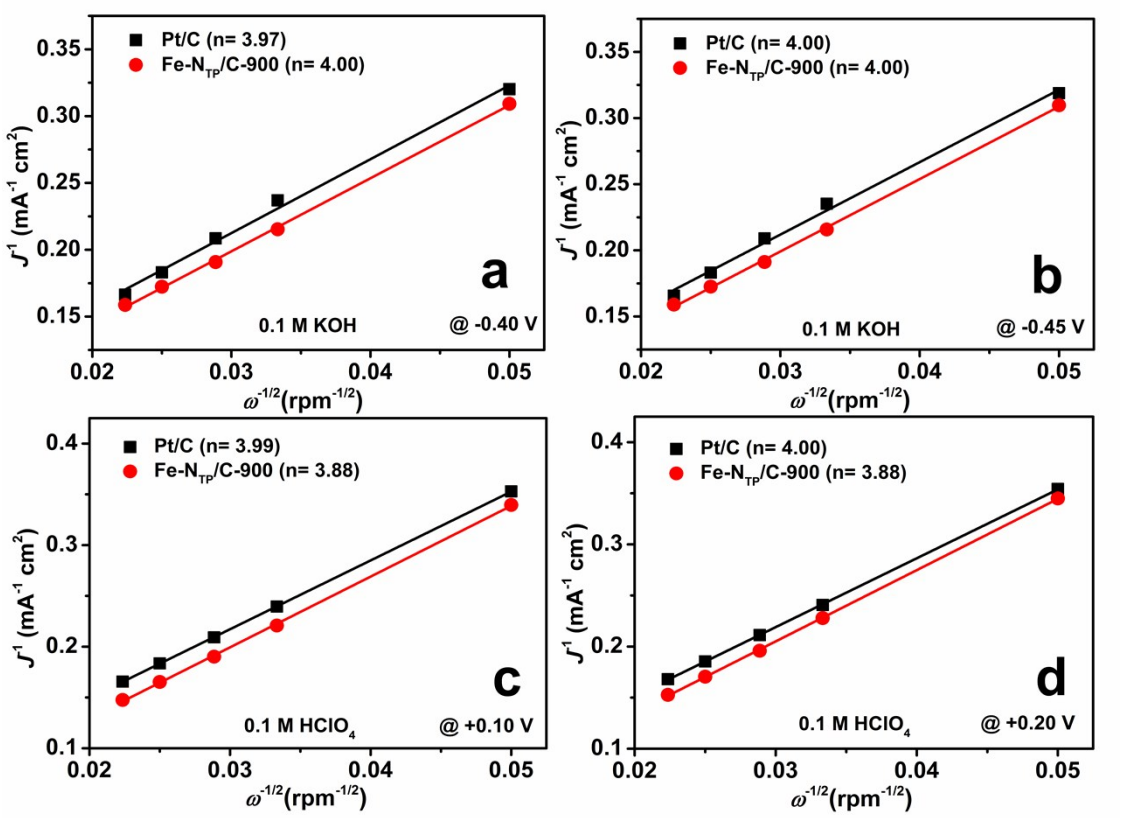

Figure S14. The K−L plots of Fe-N_{TP}/C-900 and Pt/C electrodes at −0.40 V (a) and −0.45 V (b) in O_2-saturated 0.1 M KOH. The K−L plots of Fe-N_{TP}/C-900 and Pt/C electrodes at +0.10 V (c) and +0.20 V (d) in O_2-saturated 0.1 M $HClO_4$.

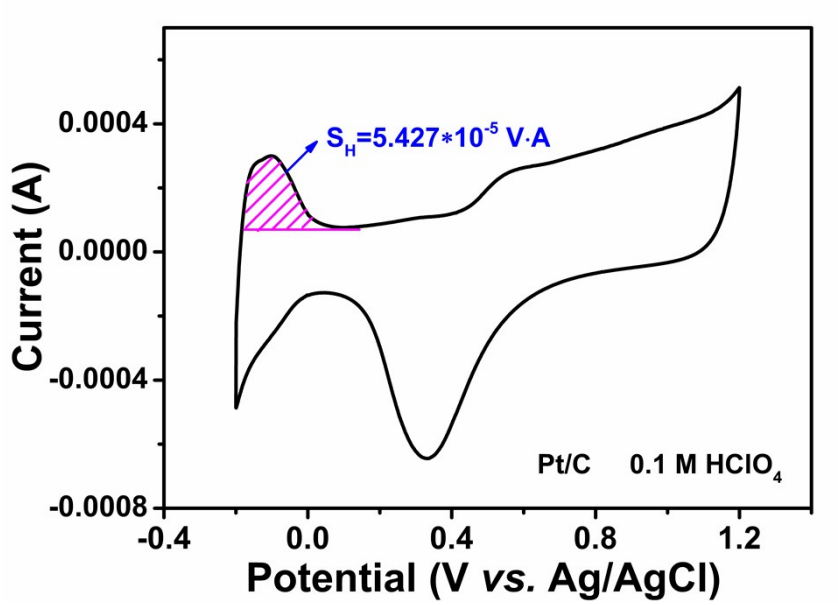

Figure S15. CV curve for Pt/C in N_2-saturated 0.1 M $HClO_4$ at a scan rate of 50 mV s^{-1}.

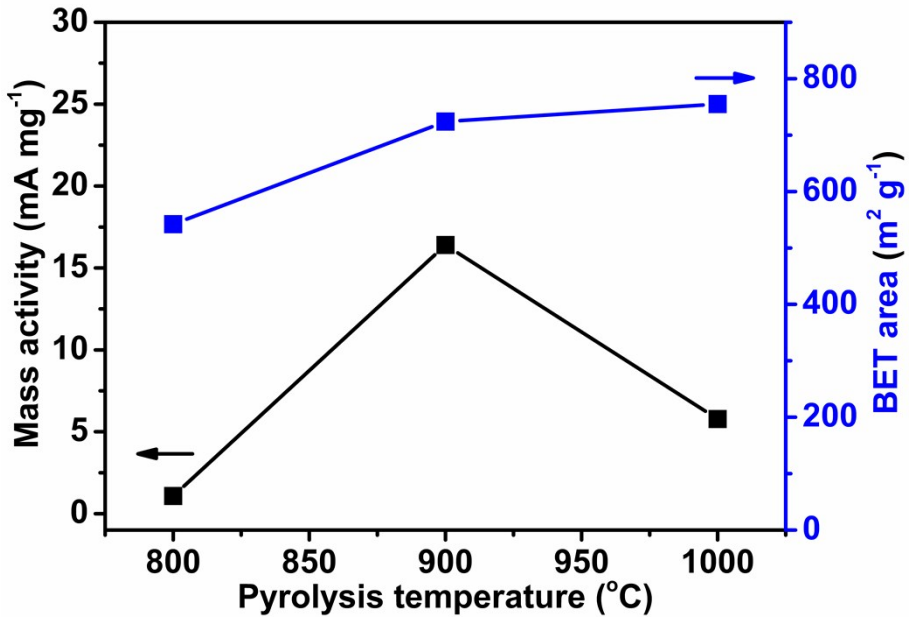

Figure S16. The dependence of mass activity (Left) and BET area (Right) on the pyrolysis temperature.

The ECSA of Pt was determined by charge integration under the hydrogen desorption peaks appearing between 0.2 and –0.2 V, by assuming a charge of 0.21 mC cm^{-2} for the electroactive Pt

surface. Then, the specific ECSA was calculated based on the following relation:

$$\text{specific ECSA} = \frac{Q_H}{m \times q_H}$$

where Q_H is the charge for hydrogen desorption, m is the Pt metal loading, and q_H is the charge required for desorbing a monolayer of hydrogen on Pt surface.

The specific kinetic current densities (j_K) associated with the intrinsic activity of the catalysts can be obtained by the following relation:

$$j_K = \frac{j_L \times j}{j_L - j}$$

Where j is the measured current density, j_K is the kinetic current density; j_L is the limited current density, respectively. The mass activity (*MA*) for Pt/C and Fe-N_{TP}/C-900 was the corresponding j at the potential of 0.55 V (vs. Ag/AgCl) in 0.1 M $HClO_4$ and –0.05 V (vs. Ag/AgCl) 0.1 M KOH.

Table S8. The specific ECSA, and mass activity for the Pt/C and Fe-N_{TP}/C-900 at a sweep rate of

50 mV s^{-1} in 0.1 M $HClO_4$ and 0.1 M KOH.

Samples	ECSA ($m^2\ g^{-1}$)	Mass activity [a] (mA mg^{-1})	Mass activity [b] (mA mg^{-1})
20 wt% Pt/C	93.3	34.1	23.5
Fe-N_{TP}/C-900	-	2.1	16.4

[a] Mass activity estimated at 0.55 V in 0.1 M $HClO_4$.

[b] Mass activity estimated at –0.05 V in 0.1 M KOH.

[a,b] The mass is the total mass of catalyst, including the carbon mass even for Pt/C. The loading of Fe-N_{TP}/C-900 is 286 μg cm^{-2}, for 20 wt% Pt/C, the loading is 143 μg cm^{-2} (28.6 μgPt cm^{-2}).

Table S9. Fe contents of Fe-N_{TP}/C-900 catalyst before and after the durability test measured by ICP-AES in O_2-saturated 0.1 M KOH electrolyte.

Fe-N_{TP}/C-900	Fe content (wt%)
before durability test	0.875
after durability test	0.822

Table S10. Summary of the electrochemical properties of various M−N/C ORR catalysts in 0.1 M KOH electrolyte.

Catalyst	E_o[a] (V)	$E_{1/2}$ (V)	J_L[b] (mA cm^{-2})	Reference electrode	Ref.
Fe-N-CNFs	–0.02	–0.14	5.40	Ag/AgCl	[2]
Fe-N/C-800	+0.923	+0.809	6.06	RHE	[3]
C-COP-P-Co	+0.9	+0.8	5.8	RHE	[4]
Fe-tpy-GO	–0.1	–0.4	3.5	Ag/AgCl	[5]
CoP-CMP800	–0.12	–0.18	4.6	Ag/AgCl	[6]
N-Fe-CNT/CNP	+1.0	+0.93	3.5	RHE	[7]
rGO/(Co^{2+}-THPP)$_7$	–0.1	–0.35	3.2	Ag/AgCl	[8]
NPC-Co45	+0.9	+0.79	5.5	RHE	[9]
Carbon-nanoshell	+0.98	+0.85	5.1	RHE	[10]
Fe-N_{TP}/C-900	+0.051 (+1.015 **vs. RHE**)	–0.055 (+0.909 **vs. RHE**)	5.79	Ag/AgCl	This work

[a] ORR onset potential in O_2 saturated 0.1 M KOH solution with the rotation speed of 1600 rpm.

[b] J_L is the limiting current density at –0.8 V (rotating speed: 1600 rpm).

References

[1] M. Yang, D.G. Yang, H.B. Chen, Y. Gao, H.M. Li, Nitrogen-doped carbon nanotubes as catalysts for the oxygen reduction reaction in alkaline medium. *J. Power Sources* 2015, **279**, 28-35.

[2] Z.Y. Wu, X.X. Xu, B.C. Hu, H.W. Liang, Y.F. Chen, S.H. Yu, Iron carbide nanoparticles encapsulated in mesoporous Fe-N-doped carbon nanofibers for efficient electrocatalysis. *Angew. Chem.*

Int. Ed. 2015, **54**, 8179-8183.

[3] L. Lin, Q. Zhu, A.W. Xu, Noble-metal-free Fe–N/C catalyst for highly efficient oxygen reduction reaction under both alkaline and acidic conditions. *J. Am. Chem. Soc.* 2014, **136**, 11027-11033.

[4] Z. Xiang, Y. Xue, D. Cao, L. Huang, J. Chen, L. Dai, Highly efficient electrocatalysts for oxygen reduction based on 2D covalent organic polymers complexed with non-precious Metals. *Angew. Chem. Int. Ed.* 2014, **53**, 2433-2437.

[5] S. Song, Y. Xue, L. Feng, H. Elbatal, P. Wang, C. N. Moorefield, G. R. Newkome, L. Dai, Reversible self-Assembly of terpyridine-functionalized graphene oxide for energy conversion. *Angew. Chem. Int. Ed.* 2014, **53**, 1415-1419.

[6] Z.S. Wu, L. Chen, J.Z. Liu, K. Parvez, H.W. Liang, J. Shu, H. Sachdev, R. Graf, X.L. Feng, K. Mullen, High-performance electrocatalysts for oxygen reduction derived from cobalt porphyrin-based conjugated mesoporous polymers. *Adv. Mater.* 2014, **26**, 1450-1455.

[7] H. T. Chung, J.H. Won, P. Zelenay, Active and stable carbon nanotube/nanoparticle composite electrocatalyst for oxygen reduction. *Nat. Commun.* 2013, **4**, 1922-1926.

[8] H. Tang, H. Yin, J. Wang, N. Yang, D. Wang, Z. Tang, Molecular architecture of cobalt porphyrin multilayers on reduced graphene oxide sheets for high-performance oxygen reduction reaction. *Angew. Chem. Int. Ed.* 2013, **52**, 5585-5589.

[9] Z.Y. Liu, G.X. Zhang, Z.Y. Lu, X.Y. Jin, Z. Chang, X.M. Sun, One-step scalable preparation of N-doped nanoporous carbon as a high-performance electrocatalyst for the oxygen reduction reaction. *Nano Res.* 2013, **6**, 293-301.

[10] Y. Wang, A.G. Kong, X.T. Chen, Q.P. Lin, P.Y. Feng, Efficient oxygen electroreduction: hierarchical porous Fe–N-doped hollow carbon nanoshells. *ACS Catal.* 2015, **5**, 3887-3893.